The Journal of Experimental Biology 208, 355-369
Published by The Company of Biologists 2005
doi:10.1242/jeb.01359



# Dynamic pressure maps for wings and tails of pigeons in slow, flapping flight, and their energetic implications

James R. Usherwood*, Tyson L. Hedrick, Craig P. McGowan and Andrew A. Biewener
*Concord Field Station, Harvard University, 100 Old Causeway Road, Bedford, MA 01730, USA*
*Author for correspondence at present address: Structure and Motion Laboratory, The Royal Veterinary College, Hawkshead Lane, North Mymms, Hatfield AL9 7TA, UK (e-mail: jusherwood@rvc.ac.uk)

*Accepted 26 October 2004*

## Summary

**Differential pressure measurements offer a new approach for studying the aerodynamics of bird flight. Measurements from differential pressure sensors are combined to form a dynamic pressure map for eight sites along and across the wings, and for two sites across the tail, of pigeons flying between two perches. The confounding influence of acceleration on the pressure signals is shown to be small for both wings and tail. The mean differential pressure for the tail during steady, level flight was 25.6 Pa, which, given an angle of attack for the tail of 47.6°, suggests the tail contributes 7.91% of the force required for weight support, and requires a muscle-mass specific power of 19.3 W kg$^{-1}$ for flight to overcome its drag at 4.46 m s$^{-1}$. Differential pressures during downstroke increase along the wing length, to 300–400 Pa during take-off and landing for distal sites. Taking the signals obtained from five sensors sited along the wing at feather bases as representative of the mean pressure for five spanwise elements at each point in time, and assuming aerodynamic forces act within the *x*–*z* plane (i.e. no forces in the direction of travel) and perpendicular to the wing during downstroke, we calculate that 74.5% of the force required to support weight was provided by the wings, and that the aerodynamic muscle-mass specific power required to flap the wings was 272.7 W kg$^{-1}$.**

Key words: aerodynamics, bird, pigeon, *Columba livia*, flight, power, lift, pressure, flapping.

## Introduction

The aerodynamic pressures, forces and power requirements of bird flight are of interest both to the engineer aiming to make flying machines, and to biologists aiming to understand either the physiology of muscle, or bird behaviour and ecology. While soaring and gliding flight can be understood within the context of conventional fixed-wing aerodynamics, appropriate analysis of flapping flight is more uncertain. Pennycuick (1975, 1989) describes adaptations of conventional fixed-wing theory for power calculations of relatively fast flapping flight, and identifies that, at lower speeds, such models are certain to run into difficulties. Pennycuick's extension of fixed-wing theory for fast flapping flight has the great merit of being somewhat predictive in nature: the power requirements for a bird flying under imagined conditions can be calculated, and so aerodynamic powers as functions of speed or loading – key factors when considering the ecology and behaviour of birds – can be predicted.

Power models considering vortex structures have been developed for animal flight (Rayner, 1979a, 1993; Ellington, 1984). Rayner develops power models based on a view of vortex structures derived from wake visualisations (e.g. Spedding et al., 1984; Spedding, 1986, 1987). However, more recent wake visualisation experiments using Digital Particle Image Velocimetry (DPIV) for bird flight under highly controlled wind-tunnel conditions (Spedding et al., 2003a,b) suggest that quite complex wake vortex structures must be considered before appropriate force balances – including the support of body weight – are achieved. Thus, while methods based on assumed vortex structures have provided one route for extending power calculations for flapping flight to slower speeds, direct methods for calculating aerodynamic powers are most appealing.

Blade-element techniques, found to be effective for propellers and helicopters, have been extended to flapping flight for hovering (Osborne, 1951; Ellington, 1984; Usherwood and Ellington, 2002a,b) and ascending (Wakeling and Ellington, 1997; Askew et al., 2001) bird and insect flight. However, these techniques are reliant on the knowledge of appropriate values of lift and drag coefficients for each, or some form of average, spanwise wing section or 'element'. These coefficients can be determined, even for revolving wings (in which case they can be quite different from steadily translating wings; Usherwood and Ellington, 2002a,b), given accurate information on wing shape and, critically, the speed and angle of incidence of the local air. While these details may be found for birds during fast flight within the confines of a wind tunnel (Hedrick et al., 2002), during which locally

induced air velocities are relatively low compared with flight or wing velocities, these techniques become progressively less reliable for flight at lower speeds. Induced velocities of the air near the wings are relatively high during slow flight, and so dynamic calculations of the angle of incidence of each wing chord to the air, and the speed of the air with respect to the aerofoil, become uncertain, resulting in unreliable calculations of time-varying aerodynamic pressures and forces from kinematic observations only.

Mechanical and mathematical modelling of aerodynamic forces and power requirements are proving effective for analysing flapping insects (e.g. Ellington et al., 1996; Liu et al., 1998; Liu and Kawachi, 1998; Dickinson et al., 1999; Wang, 2000; Ramamurti and Sandberg, 2002; Sun and Tang, 2002; for a review of insect techniques, see Sane, 2003). However, the relative complexity of vertebrate wing morphology and kinematics has limited mechanical model approaches, and numerical computational fluid dynamics approaches are currently additionally limited by the computing power required for 3-dimensional, unsteady flows at higher Reynolds numbers.

Measurement of the forces and strains experienced by the major flight muscles of birds (the pectoralis) allows direct calculation of the mechanical power requirements, which include both the inertial power associated with accelerating the wings and the aerodynamic power (Biewener et al., 1998; Tobalske et al., 2003; Hedrick et al., 2003). While this technique has considerable appeal, as it gives a direct indication of the force requirements of the pectoralis, and may allow relative, if not quantitative, changes in power requirements to be determined (e.g. Tobalske et al., 2003), the calibration of pectoralis-induced bone strain recordings to provide reliable forces over the full range of wing motion can be problematic. This arises from the fact that *in situ* simulations of muscle force transmission used to calibrate force *via* a bone strain gauge mounted on the deltopectoral crest (DPC) of the humerus are sensitive to the direction of muscle pull and the bending moment applied to the DPC.

We present in the current study a novel experimental approach for determining the contributions of the wings and tails of pigeons in slow flight to weight support, and their aerodynamic power requirements. Pressure transducers can be applied between or through bird feathers (developing on from Usherwood et al., 2003) to provide measurements of differential pressures at a range of points along and across wings and tails. Using these point pressures as representative of pressures for appropriate sections, the aerodynamic forces on wings and tail can be inferred. With simple kinematic measurements of orientation and velocity, the aerodynamic power requirements associated with aerodynamic forces on wings and tails can then be calculated.

## Materials and methods

### *Overview*

Six similar pigeons (wild-type *Columba livia* Gmelin 1789 purchased from a licensed animal dealer), three used for the acceleration-compensated pressure experiments (Table 2), and three used for the eight-site wing-map experiments (Table 3), had accelerometers and differential pressure sensors attached at a range of sites. For each arrangement of sensors, each pigeon was required to fly between two perches separated by 7 m located in a hallway (1.9 m wide, 12 m long, 4.2 m high), while towing a pair of light (9.9 g $m^{-1}$), 6-strand shielded signal cables (NMUF6/30-4046SJ; Cooner Wire, Chatsworth, CA, USA). These flights were relatively brief, consisting of approximately 18 wing beats, and were achieved without apparent difficulty. In every arrangement of sensors, an accelerometer was positioned at the base of an outer secondary feather (S3). This accelerometer provided a synchronising signal, allowing the measurements from different trials, and different sensor arrangements, to be combined. This technique was used throughout in order to allow the compilation of a pressure map for many sites along and across the wing and tail, while loading each pigeon with only two differential pressure sensors (and a range of accelerometers) for any single flight. Each wing stroke cycle was defined by the peak in accelerometer signal, relating to rapid upwards acceleration of the wing towards the end of downstroke. The time-base for each raw signal was normalised to the wing stroke cycle, thus slight differences in frequency do not result in increasing variation in measurement through the cycle. The signals from each trial were split into (i) a take-off flap followed by three full flaps, (ii) three full flaps at the middle of the flight, and (iii) three full flaps prior to landing followed by a landing flap. This synchronising accelerometer trace is shown in green (black lines show ± 1 S.D.) at the bottom of Figs 3–7.

The signals used to provide the mean ± S.D. (for $N$=3 pigeons) for each sensor position for each pigeon are means of 15–20 flights; the S.D.s indicate variability among pigeons (and applications of the sensors), not the variability from flight to flight.

### *Sensors and sensor attachment*

Two small, disc-shaped (diameter=6.4 mm, depth=2.6 mm) differential pressure sensors (Entran EPA-EO1-2P, ± 2PSI full range; Entran Devices Inc., Fairfield, NJ, USA) each had a pen-nib glued with epoxy over the single gauge-port, resulting in a unit with a mass of 0.5 g and the shape of a thumb-tack or drawing pin. At the most distal pressure sensor site (see below), the sensor mass contributed an additional 13% to the wing moment of inertia (taking the value of $172.7\times10^{-6}$ kg $m^2$ for the moment of inertia of a pigeon wing from Van den Berg and Rayner, 1995). The hollow pen-nib (of length 4.4 mm) provided a conduit through which pressures could be transmitted to the membrane in the sensor unit. The nib was also narrow enough (0.64 mm o.d.) to be inserted through feather shafts, and held firmly (though reversibly) in place with hot-glue with minimal disruption to the feather. When attached through a feather shaft, the pen-nib projects a little way through the dorsal surface of the tail or wing, and the disc of the sensor body lies flat along the ventral surface. A difference in pressure

between the upper surface, to which the pen nib is exposed, and the ventral wing surface, to which an array of holes on the flat bottom of the sensor is exposed, results in a deflection of the membrane in the sensor, and the production of a voltage signal.

Two ±250 ***g*** accelerometers (Entran EGAX-250) of dimensions 4 mm×4 mm×7.5 mm, and two ±50 ***g*** accelerometers (ICSensors 3031-050; San Jose, CA, USA) had 7 mm steel pins mounted with epoxy glue at the centre of the sensor, parallel to the direction of sensitivity (individual masses of 0.8 g and 0.5 g, respectively). These pins could then be inserted through a feather shaft and held in place with hot-glue, firmly mounting the accelerometers directly underneath the same feathers that carried the pressure sensors (Fig. 1).

Signals from pressure sensors and accelerometers were amplified and recorded at 5000 Hz using National instruments hardware (SCXI-1000DC, National Instruments, Austin, TX, USA). All signals were collected, digitally filtered (150 Hz recursive Butterworth – 19 times the wingbeat frequency), calibrated and analysed using National Instruments LabVIEW 5.1.

The sensitivities of the differential pressure sensors to acceleration were determined by attaching the sensors to the tip of a modified fan blade of length 0.22 m, and ramping the fan speed from zero to approximately 5.6 cycles $s^{-1}$ and back down again. During this, the pressure sensor being tested was enclosed in a rigid case so that air around the sensor was always still with respect to the sensor. Power and signal connections ran from the sensor to the centre of rotation of the fan *via* a 4-channel mercury slip ring (Mercotac 430, Carlsbad, CA, USA) to the amplifiers and recording equipment. The frequency of rotation of the fan was identified from the cyclic variation due to gravity: with the fan orientated vertically the acceleration experienced by the sensor oscillated with an amplitude of 1 ***g*** on top of the signal imposed due to centripetal accelerations (up to 160 ***g***, around double the peak observed at the base of the feather P8). With this set-up, the response of each pressure sensor to acceleration was measured, and found to be linear and of magnitudes of 1.0 and 1.2 Pa $g^{-1}$.

### *Transducer placements*

Accelerometers and pressure sensors were attached through feather shafts while each pigeon was blindfolded and calm; anaesthesia was never required. For all placements of the pressure sensors along the wing, the pen-nib projected through the feather shaft, and then through a small (approximately 5 mm×5 mm) tab of surgical adhesive tape, which prevented nearby feathers from flicking over the port during flight. Wires to the transducers were controlled, where necessary, with ties of thin cotton thread sewn through unused feather shafts. Excess transducer wire was collected on the back of the pigeon and held in place with tape. The total load of all transducers, signal wires and tape was approximately 15 g, <4% of body mass. The connection between the sensor wires and the pair of 6-lead shielded cables was also located on the back and acted as a mechanical fuse in case of snagging of the cables. The 6-lead cables (carrying a total of two supply lines and five pairs of signal wires) were arranged so that each passed around one side of the body between the wings and the tail, from where the two cables joined again beneath the pigeon. This arrangement permitted a full range of movement for both the wings and the tail, which were able to spread fully.

The acceleration-compensated trials involved three sets of transducer placements (Table 1; Fig. 1A,B). The first set had pressure sensors and accelerometers on the outer tail, located on the second from outermost feathers [i.e. rectrice conventionally termed R5 – pigeons have 12 rectrices from 1 (central pair) out to R6 (outermost pair)]. The second set had sensors on the 'inner tail', located on the 5th tail feathers in from outermost (R2). At these inner tail placement locations, a few under tail coverts were trimmed to prevent the ventral ports from being blocked. The third set of transducer placements were on the right wing (Fig. 1B), one pressure

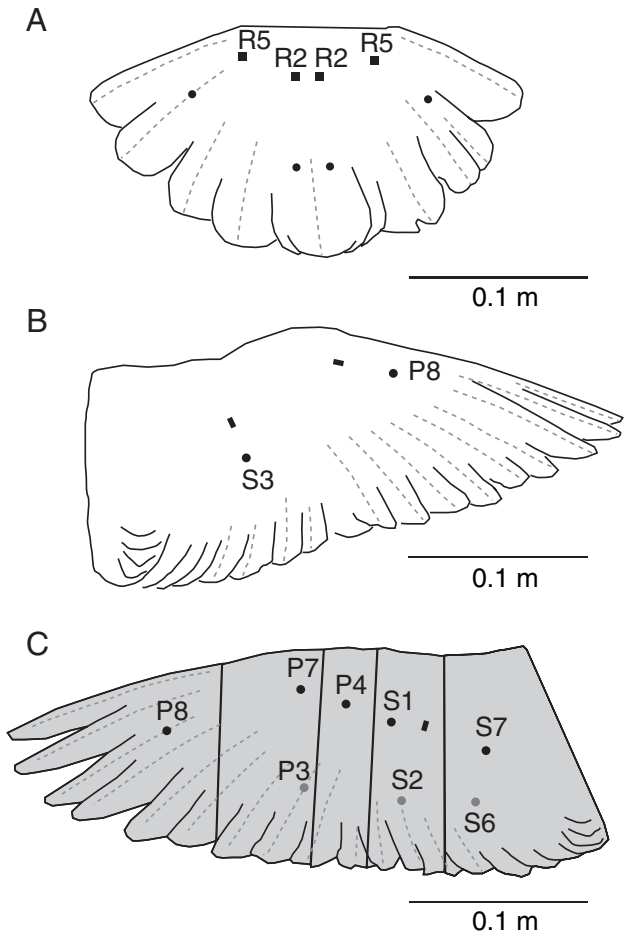


Fig. 1. Positioning of accelerometers (rectangles) and differential pressure transducers (circles) across (A) tail, (B) wing for acceleration-compensated trials, and (C) the non-compensated 8-position map. Following convention we code our feathers R for rectrices (tail feathers), P for primaries and S for secondaries, with numbering for the wing feathers counted from the primary/secondary boundary. The pressures measured at each of five positions along the leading edge are taken as representative for the wing sections demarcated by straight lines in C.

Table 1. *Transducer placements*

| | Differential pressure sensors | | Accelerometers ±250 g | | Accelerometers ±50 g | |
|---|---|---|---|---|---|---|
| | A | B | A | B | A | B |
| Acceleration-compensated experiments | | | | | | |
| Inner tail | Left inner tail (R2), mid-feather | Right inner tail (R2), mid-feather | X | Right S3* base | Left R2 base | Right R2 base |
| Outer tail | Left outer tail (R5), mid-feather | Right outer tail (R5), mid-feather | X | Right S3* base | Left R5 | Right R5 |
| Right wing | P8, 25 mm from base | S3, 25 mm from base | Right P8 base | Right S3* base | X | X |
| Non-acceleration-compensated experiments | | | | | | |
| P8P7 | Left P8 mid | Left P7 base | (Right P8 base) | (Right S3 base) | Left S3* base | X |
| P4P3 | Left P4 base | Left P3 mid | (Right P8 base) | (Right S3 base) | Left S3* base | X |
| S1S2 | Left S1 base | Left S2 mid | (Right P8 base) | (Right S3 base) | Left S3* base | X |
| S6S7 | Left S6 mid | Left S7 base | (Right P8 base) | (Right S3 base) | Left S3* base | X |

R indicates a rectrice (tail feather), with numbers indicating feathers (of 6) from the centre. P indicates a primary feather, S indicates a secondary feather, and numbering counts from the primary/secondary boundary (thus, given there are 10 visible primaries in an adult pigeon wing, P8 is the third visible primary from the wing tip).

S3* indicates the synchronising accelerometer. X indicates the sensor was not used for a given set-up. Values from sensors shown in parentheses (those on the right wing for non acceleration-compensated experiments) were measured but are not discussed here.

sensor/accelerometer pair on the third primary from the most distal (as primaries are conventionally numbered from proximal to distal, and there are ten visible primaries on an adult pigeon wing, this is termed P8), and one pair on the third secondary from the most distal secondary (secondaries are conventionally counted from distal to proximal, thus this is S3).

The non-acceleration-compensated trials involved measurements obtained from four sets of pressure sensor placements (Table 1; Fig. 1C) for each pigeon. By time-normalising (allowing wingbeats of slightly different period to be combined) and synchronising with the accelerometer on S3 (to identify a consistent part of the wingbeat cycle), we were able to develop a pressure map of eight sites along and across the wing (Fig. 1C) for multiple wingbeats of take-off, slow level and landing flight.

### *Video and kinematics*

Two flights were filmed at 250 frames $s^{-1}$ (Photron Fastcam-X 1280 PCI; Photron USA Inc., San Diego, CA, USA) for each pigeon and sensor positioning. For the acceleration-compensated experiments, the camera was placed at 8 m lateral to the line of flight, to give a perpendicular lateral view of the middle of the flights, from which tail angles $\alpha_{tail}$, flight velocities $V$, and the inclination of the stroke plane to the horizontal $\beta$ were calculated (Fig. 2A). For the non-acceleration-compensated experiments the camera was placed 4.8 m beyond the landing perch, providing a view of the middle portion of flight at a distance of 8.3 m. From this view the angle of the left wing, taken as the angle subtended between a line from the shoulder to the alula, and the horizontal, was measured for the downstroke of the three middle flaps of each flight filmed. We term this the downstroke angle $\phi_{x\text{-}z}$, indicating it is the projection of the downstroke angle $\phi$ on to the $x$–$z$ plane (Fig. 2B). Given the relatively large distance between camera and subject, we ignore parallax effects for both camera positions.

### *Weight support and power requirements from the tail*

The precise pressure distribution along and across the tail is currently unmeasurable. However, if the differential pressure measurements for outer and inner sites are averaged, and $\overline{dP_{tail}}$ taken as representative for the whole tail surface $S_{tail}$, which is then considered as flat and inclined at an angle $\overline{\alpha_{tail}}$, the aerodynamic force from the tail can be calculated, and the force components in the direction of weight support $\overline{F_{z,tail}}$ calculated assuming that the force acts perpendicular to the thin surface:

$$\overline{F_{z,tail}} = \overline{dP_{tail}} S_{tail} \cos(\overline{\alpha_{tail}}) . \quad (1)$$

Similarly, the aerodynamic force from the tail opposing the direction of motion of the pigeon can be calculated. Given a flight velocity $V$, this results in a power requirement $P_{tail}$ for pulling the tail along:

$$P_{tail} = \overline{dP_{tail}} S_{tail} \sin(\overline{\alpha_{tail}}) V . \quad (2)$$

The manner in which this power requirement should be considered within the conventional framework is unclear, as $P_{tail}$ cannot be simply assigned to parasite, profile or induced powers.

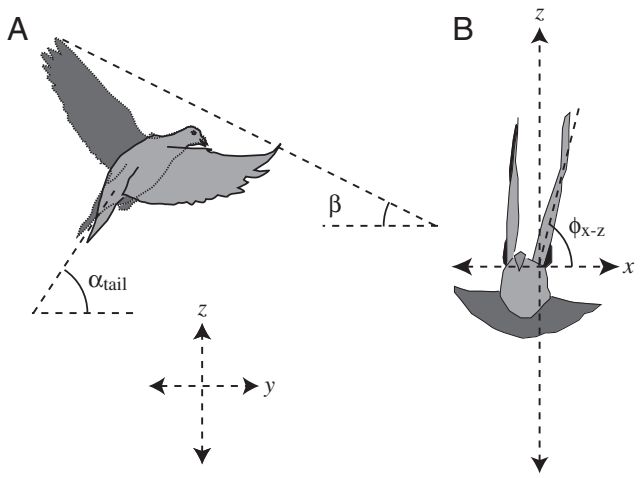


Fig. 2. The axes and measured angles for side view (A) and front view (B) during level flight between two perches. For an explanation of symbols, see List of symbols.

The force per unit area is conventionally related to air density ρ (taken to be 1.2 kg $m^{-3}$), wing area and velocity with the use of force coefficients, in this case the resultant force coefficient $C_R$. Using the same assumptions as above:

$$dPS = \frac{\rho}{2} C_R S V^2 . \quad (3)$$

Thus,

$$\overline{C_{R,tail}} = \frac{2dP}{\rho V^2} . \quad (4)$$

The vertical (lift) and horizontal (drag) components of the resultant force coefficient, $C_{L,tail}$ and $C_{D,tail}$ respectively, are given by the cosine and sine of $\overline{\alpha_{tail}}$, as in Eq. 1 and 2. The values we describe are the means obtained for the three pigeons, derived from differential pressures averaged from all four tail sites over the whole period of the three 'middle' wingbeats of each bird.

### *Weight support from the wings*

If the measured pressures for similar chordwise sites (we take the five sites located towards the leading edge of the wing) can be taken as representative of the mean pressures for appropriate section areas (Fig. 1), then the aerodynamic forces on each wing element, and so on the whole wing, can be calculated. At each instant, each wing element of area $S$ and measured differential pressure $dP$, the aerodynamic force $F'$ is simply

$$F' = dPS . \quad (5)$$

Assuming that the net aerodynamic force for each section acts perpendicular to the wing surface – an incorrect but close assumption for attached flow, and very close to true for detached flow and high force coefficients (Dickinson, 1996; Dickinson et al., 1999; Usherwood and Ellington, 2002a) – then, with an outstretched, untwisted wing in which all wing chords are horizontal (appropriate for downstroke), the vertical force contribution from each wing element $F_z'$ can be calculated:

$$F_z' = F'\cos(\phi_{x\text{-}z}) . \quad (6)$$

During upstroke, the differential pressures are slight (Fig. 3), and the wing is brought close to the pigeon's body during slow flight (Fig. 7d). Thus, although some degree of weight support may be achieved during the upstroke, it is unlikely to be large. Further, our kinematic data do not provide sufficient resolution to indicate upstroke weight support accurately from the pressure measurements. Because of this we assume that weight support from the wings occurs entirely during the downstroke during slow, level flight. For a pair of wings over a complete cycle time 1/$f$, adding the contribution of each (of five) wing sections from the wing base ($r$=0) to the wing tip ($r$=$R$), where $r$ is the distance from the shoulder and $R$ is the wing length, and over the duration of the downstroke (ds; from $t$=0 to $t$=$T_{ds}$, the period of the downstroke), the mean vertical force from the wings $\overline{F_{z,wings}}$ is given by:

$$\overline{F_{z,wings}} = 2f \int_{t=0}^{t=T_{ds}} \sum_{r=0}^{r=R} F'\cos(\phi_{x\text{-}z}) , \quad (7)$$

where each element has an area $S_r$, and the wing angle with respect to the horizontal (projected on to the $x$–$z$ plane) varies as a function of time ($\phi_{x\text{-}z}$). It should be noted that, in order to cover the entire wing within the constraints of successful transducer positioning, the five section areas are somewhat arbitrary (Fig. 1C), and the sensors, while at relatively consistent chordwise positions, are not in the centre of each section.

During level flight, the loaded body weight of the pigeon should be completely supported by aerodynamic means. Consequently, determining the percentage of weight support achieved by the vertical components of force calculated for both the wings and the tail provides a check on the accuracy of the force calculations obtained from our differential pressure measurements.

### *Calculating aerodynamic power from differential pressure measurements*

Given the same assumptions as those used above in the calculation of weight support, that a point pressure measurement is representative of an average section pressure, and that the resultant aerodynamic force acts against the motion of the wing in the $x$–$z$ plane (because the forces act perpendicular to the wing section, and each chord is horizontal), then a direct calculation of the mean aerodynamic power $\overline{P_{aero}}$ required to move the wing can be made:

$$\overline{P_{aero}} = 2f\dot{\phi}_{x\text{-}z} \int_{t=0}^{t=T_{ds}} \sum_{r=0}^{r=R} F'r . \quad (8)$$

While some aerodynamic forces may be acting in different directions – for instance as thrust overcoming body drag – and there is certainly motion of the wing out of the $x$–$z$ plane, it

appears reasonable, at least for slow flight, to expect the dominating force on the wings to be associated with weight support, and the dominating force requirement of the pectoralis to be to pull the wing down.

The effective moment arm $R_{\text{eff}}$ of the total aerodynamic force on the wing, or the distance of the centre of pressure from the shoulder, can be a useful term for understanding the derivation of power requirements. As a proportion of wing length,

$$\frac{R_{\text{eff}}}{R} = \frac{\sum F' r}{R \sum F'} . \quad (9)$$

Thus, a value of $R_{\text{eff}}/R$=0.5 indicates that the centre of pressure is halfway between shoulder and wingtip. Also, the power for both wings at any instant can then be described as:

$$P_{\text{aero}} = 2\dot{\phi}_{\text{x-z}} \left( \frac{R_{\text{eff}}}{R} \right) R \sum F' . \quad (10)$$

It should be noted that the aerodynamic powers calculated in this manner ought not to be considered separately from the traditional divisions of aerodynamic power: if profile, parasite and induced powers could be calculated correctly, their sum should result in the power required to drive the wings through the air. It is this power that we calculate using the differential pressure measurements.

## Results

The two sets of three pigeons used for the acceleration-compensated pressure map of the tail and two wing sites (Table 2) and for the non-compensated 8-point pressure map of the wings (Table 3) are similar both morphologically and kinematically: mean unloaded masses were within 5% (0.468 and 0.445 kg, respectively); mean wing spans within 0.6%; and mean wingbeat frequency within 0.5%. The synchronising accelerometer trace (green lines in Figs 3–7, ±1 S.D. shown by black lines) from an accelerometer placed at the base of secondary S3 allows signals from separate flights to be combined. Each flap cycle is defined by the peak in accelerometer signal, relating to rapid upwards acceleration of the wing towards the end of downstroke. Underlying vertical grey bars indicate periods of downstroke. These downstroke periods are defined from kinematics for the level flaps. For take-off and landing, downstroke is assumed to relate to a positive differential pressure measured at the primaries.

### *Acceleration compensation*

Acceleration compensation has relatively little effect on the differential pressure signals for inner and outer tail positions, and even the two wing positions (Figs 3 and 4). During level flight (Fig. 4), a consistent deviation is

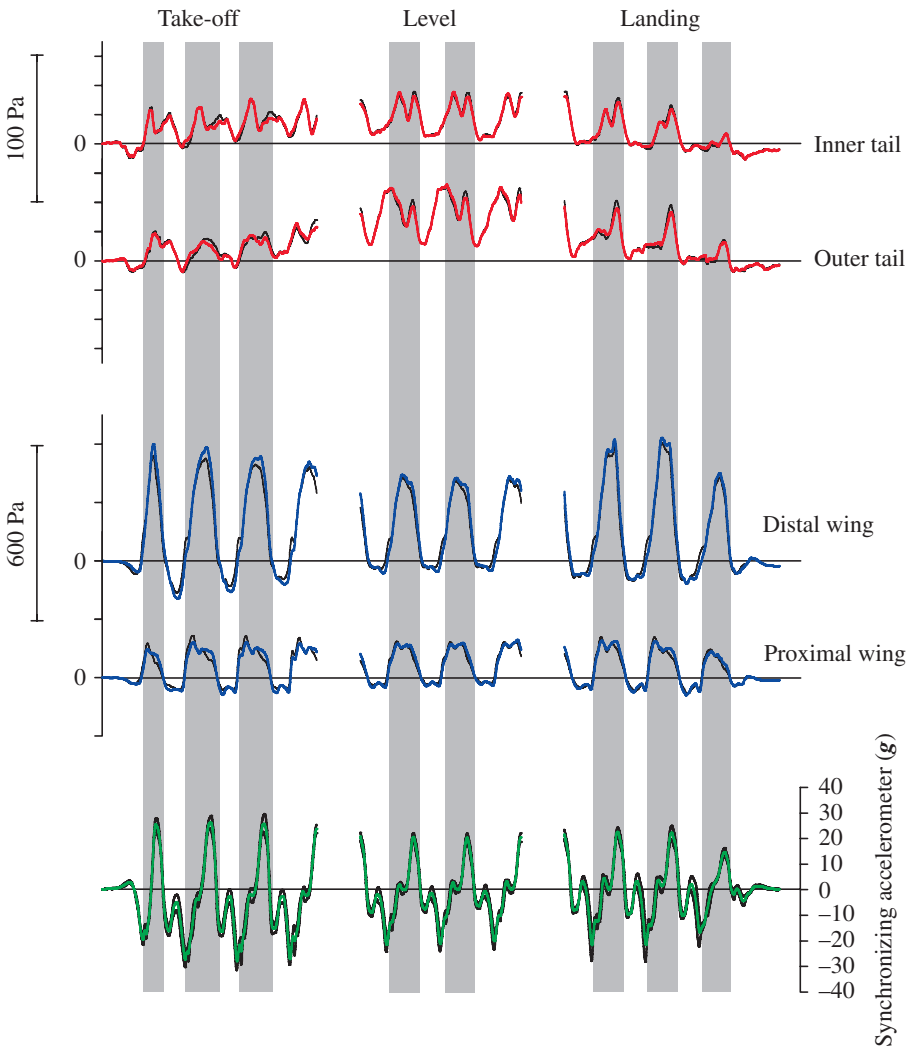


Fig. 3. Average acceleration-compensated pressure measurements for inner and outer tail positions (red lines) and two positions along the wings (blue lines), with non-acceleration compensated results (black lines) underlying. The synchronising accelerometer trace (green lines throughout; black lines indicate ±1 S.D.; *N*=3 pigeons) from an accelerometer placed at the base of secondary S3 allows signals from separate flights to be combined; each cycle is defined by the peak in accelerometer signal, relating to rapid upwards acceleration of the wing towards the end of downstroke. The time-base for each raw signal is normalised to the wing stroke cycle (thus slight differences in frequency do not result in increasing variation through the cycle). In each trace, the signal is split into a take-off flap followed by three full flaps, three full flaps at the middle of the flight, and three full flaps prior to landing followed by a landing flap. Underlying grey bars indicate periods of downstroke throughout.

Table·2. *Morphology, kinematics and results for acceleration-compensated experiments*

| | |
|---|---|
| Loaded mass $m$ (kg) | 0.483±0.027 |
| Wing span $b$ (m) | 0.660±0.01 |
| Frequency $f$ (Hz) | 8.02±0.69 |
| Flight velocity $V$ (m $s^{-1}$) | 4.46±0.27 |
| Tail angle of attack $\overline{\alpha_{tail}}$ (deg.) | 47.6±6.4 |
| Inclination of wing stroke plane $\beta$ (deg.) | 35.1±2.6 |
| Tail area $S_{tail}$ ($m^2$) | 0.0204±0.0020 |
| Differential pressure: inner tail (Pa) | 18.2±1.0 |
| Differential pressure: outer tail (Pa) | 32.9±4.5 |
| Differential pressure: mean $\overline{dP_{tail}}$ (Pa) | 25.6±8.5 |
| Weight support % | 7.91±2.5 |
| Direct power (W) | 1.70±0.2 |
| Body mass specific power (W $kg^{-1}$) | 3.68±0.58 |
| Muscle mass specific power (W $kg^{-1}$) | 19.3±3.0 |
| $\overline{C_{R,tail}}$ | 2.14 |
| $\overline{C_{L,tail}}$ | 1.44 |
| $\overline{C_{D,tail}}$ | 1.59 |

Values are means ± S.D. ($N$=3).

The muscle mass used for the muscle mass specific power calculation is that of the pair of pectoralis muscles (18% body mass); while the power costs here are due to the tail, they are largely 'paid' for by the wing-flapping musculature.

Table 3. *Morphology and kinematics for non-acceleration-compensated experiments*

| | |
|---|---|
| Loaded mass $m$ (kg) | 0.460±0.040 |
| Wingspan $b$ (m) | 0.664±0.02 |
| Frequency $f$ (Hz) | 7.98±0.46 |
| Wing length $R$ (m) | 0.302±0.022 |
| Single wing area ($m^2$) | 0.0296±0.0054 |
| Kinematic means for 3 middle flaps | |
| Peak upstroke angle $\phi_{x\text{-}z,max}$ (deg.) | 86.2±7.5 |
| Angular velocity $\dot{\phi}_{x\text{-}z}$ (deg. $s^{-1}$) | –2023±60 |
| Downstroke time $T_{ds}$ (s) | 0.0673±0.0023 |

Values are means ± S.D. ($N$=3).

identifiable at the distal wing site during the 'clap' at the end of upstroke/beginning of downstroke, a period of high acceleration (up to 80 $\boldsymbol{g}$) and relatively low differential pressure. A second consistent deviation between acceleration-compensated and non-compensated pressure measurements, though in the opposite direction and of smaller proportional significance, occurs towards the end of downstroke. During this time, the wing is rapidly decelerating (accelerating upwards; note the accelerometer trace) as the wing slows towards the end of downstroke. Generally, though, non-acceleration compensated signals provide an adequate representation of the differential pressures. This supports the use of our more detailed 8-site non-acceleration-compensated pressure map of the wing for interpreting the aerodynamic forces developed under these flight conditions.

### *Tail lift, drag and power*

The average differential pressure across the tail for a whole wing stroke cycle increases during take-off, is level during the middle three flaps, and reduces as the pigeons come into land (Fig. 3). The tail is widely spread during all of the flight between the two perches, and it is held at a high angle to the direction of travel (Table 2). While any contribution to weight-support during slow flight may be valuable, the angling of the tail near to 45° suggests that the tail acts as a poor lifting surface with a lift:drag ratio of ~1.0, thus any benefit from contributing to weight support may be offset by an increase in drag; the tail, at least at these low speeds, does not act as an efficient weight-supporting fixed wing. Instead, the tail orientates the net aerodynamic force vector required from the wings forwards: the wings are required to produce less force supporting weight, but a greater thrust force to overcome the tail drag. Thus, one effect of the tail is that the wings are required to act in a more propeller- (*versus* helicopter-) like manner.

A power requirement for pulling the tail through the air can be calculated assuming that the mean pressure from the four measured sites during level flight (Fig. 5) acts across the whole surface, and the net aerodynamic force acts perpendicular to the tail (Table 2). We do not suggest that this power is contributed by the tail musculature; rather, the aerodynamic drag due to the tail may be treated as a large parasite drag. However, due to some contribution to weight support, tail-drag contributes somewhat to the traditional 'induced drag' term. Whatever the distribution of tail-drag between conventional drag terms, the power required to pull the tail through the air is likely to be contributed by muscles that flap the wings, dominated by the pectoralis muscles.

### *Wing pressures*

The mean (± 1 S.D. shown in black, $N$=3 pigeons) non-acceleration-compensated differential pressure signals for eight positions along and across the wing (Fig. 1C) are shown for take-off, level and landing flight (Fig. 6). While distal sensor placements measure peak differential pressures that are higher during take-off and landing than level flight, this is not the case for more proximal positions. For the innermost site, on secondary S7, peak pressure differential is slightly higher during the level flaps than take-off and landing. This agrees with the observations of take-off flight in geese (Usherwood et al., 2003), and matches expectations for flapping wings, that distal sites are required to produce relatively high aerodynamic forces during slower flight, and proximal sites, with the lower flap velocities, contribute lift forces during higher speed flight. Negative pressures (indicating relatively higher pressures on dorsal surfaces than ventral) are observed at all sites during take-off and, to a lesser extent, during landing. This confirms that the upstroke can contribute aerodynamic forces during slow flight in the pigeon with a change in sense of circulation (Alexander, 1968). It appears reasonable to infer that these forces are beneficial, as negative pressures *could* be avoided with slight

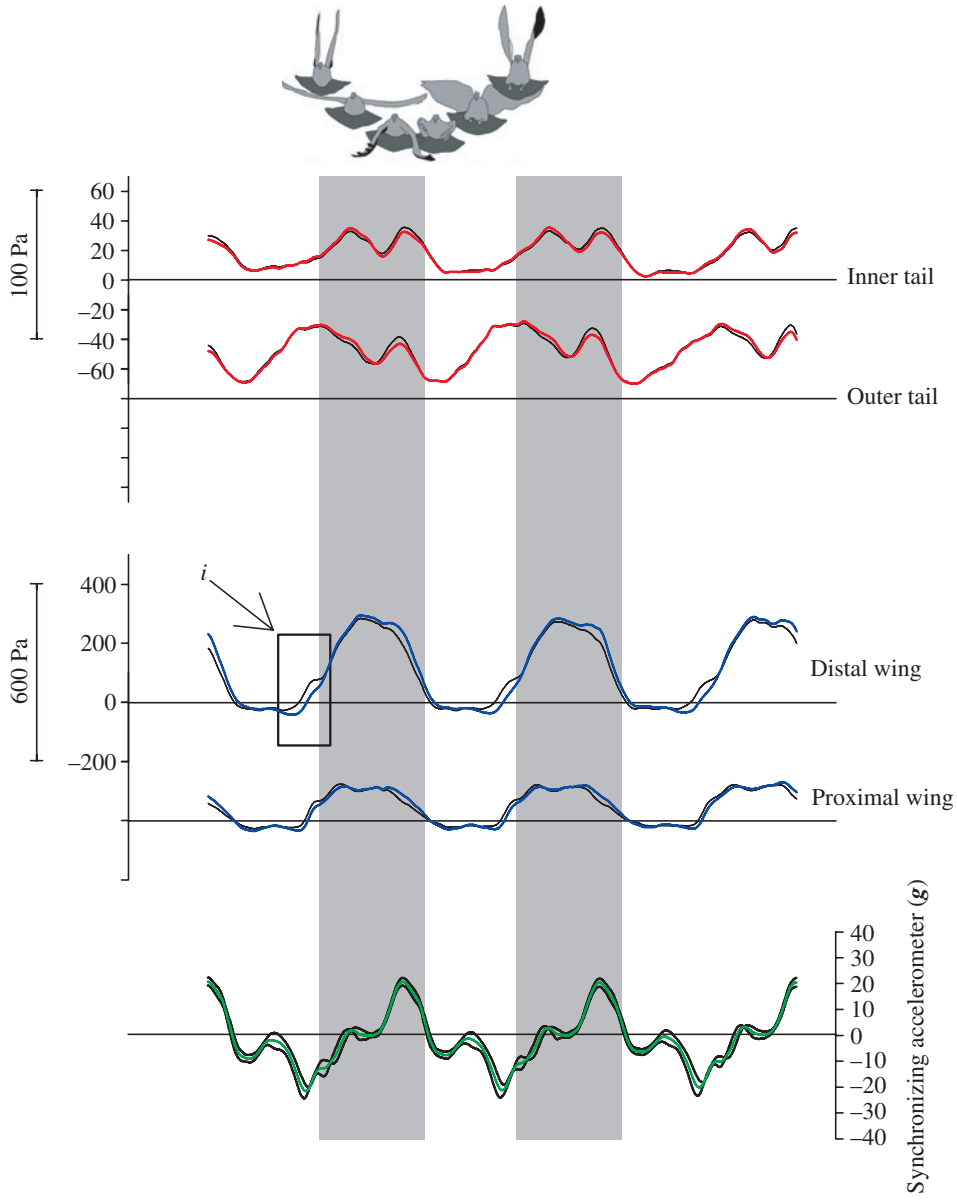


Fig. 4. An expansion of Fig. 3 for the middle three flaps only, with traced kinematics of the wing stroke included. The effect of acceleration is highlighted (*i*) for the distal wing position, and relates to the high acceleration (up to 80 ***g***) at the 'clap' at the upstroke/downstroke transition. The effects of acceleration-compensation are generally slight for both tail and wing differential pressure signals.

changes in either the degree of supination or the path of the wing during upstroke.

The development of pressure with time during level flight is related to outline tracings (Fig. 7), each separated by approximately 16 ms. More distal sites show higher amplitude signals than more proximal sites, consistent with their higher flapping velocities (Fig. 8A,C). Higher section velocities may increase section pressure differentials both by increasing the angle of incidence of the section to the air (increasing the section force coefficient), and increasing the relative air velocity, thus raising the pressure differential for a given force coefficient. While, at the very end of downstroke the wings supinate [placing each wing chord at an angle to the horizontal (see Fig. 2A)], the wing chords are approximately horizontal throughout the majority of downstroke (Fig. 7a–c). Thus, the wing chords are approximately horizontal during most of the wing motion during which significant pressure is developed.

### *Wing forces and powers*

Fig. 8 shows a development of the implications of the differential pressure measurements and the downstroke kinematics, leading to calculations of weight support and aerodynamic power. The five sites towards the leading edge of the wing (P8, P7, P4, S1 and S7), having similar chordwise positions, are included in our analysis. Two of the middle three flaps are shown, as flap cycles have to be complete for calculations of mean weight support and power. During downstroke, the wing stroke angle (Fig. 8B) varied linearly with time within the *x*–*z* plane ($\phi_{x\text{-}z}$) (i.e. observed from front-on as the animal flew toward the camera, Fig. 2), indicating a curvilinear change of downstroke angle within the stroke plane, due to the inclination of the stroke plane from the horizontal by an angle $\beta$ (35°; Table 2). Variation in downstroke angle was calculated using the mean kinematic variables given in Table 3. The geometric velocity (including forward flight speed, and taking into account the inclination of the stroke plane) for each wing section (Fig. 8C), shows that variation in differential pressures is broadly related to section speeds. Mean section forces (Fig. 8D) were determined assuming that the measured point pressures can be taken as mean pressures for relevant wing sections of known area. These section forces were then combined, and their orientations to the vertical taken into account when calculating their contribution to vertical weight support (Fig. 8E).

Muscle-mass specific aerodynamic powers calculated from point differential pressure measurements are shown as a function of the wingstroke cycle (Fig. 8G) and averaged for appropriate stroke-cycle periods (Table 4). Muscle-mass specific powers are calculated assuming that the pectoralis dominates downstroke power and constitutes 18% of body

mass (Dial and Biewener, 1993; Biewener et al., 2998; Soman et al., 2005). Means ± S.D. for vertical weight support, effective aerodynamic moment arm, and powers are calculated from appropriate individual average measurements of differential pressure, kinematics and morphology, with inter-individual averages only determined as the final step.

## Discussion

### *Tail pressures and aerodynamic mechanisms*

A double peak in differential pressure (positive indicating a ventral to dorsal direction) is evident each downstroke, although the relative magnitudes of the two pressure peaks during downstroke changes through the flight (Fig. 3): during take-off, the earlier peak is slightly larger; during the three level flaps, the peak values are similar; and during landing the second peaks increase in magnitude. Acceleration-compensated pressure measurements across the tail and two wing sites, along with accelerometer signals, are related to tracings of the wingstroke cycle in Fig. 5. Differences are observable between inner and outer sites during the first peak. The cause of this first peak is uncertain, but may include a slight increase in incidence of the tail due to a movement of the tail with respect to the body, or some influence of the wake from the wings during the first half of downstroke. The cause of the second pressure peak is clearer. It occurs towards the end of downstroke, when the wing is accelerating strongly upwards (slowing the downstroke); the vertical red broken lines (Fig. 5) show that these peaks in both inner and outer tail pressure are correlated with the upward acceleration of the wings toward the end of downstroke and a concurrent downward acceleration of the tail. During this period of diminishing aerodynamic forces from the wings, the acceleration of the mass of the wings results in a counter-acceleration of the body and tail: a negative acceleration is observed (Fig. 5, second pair of traces) from the accelerometers at the base of the tail, indicating a downwards

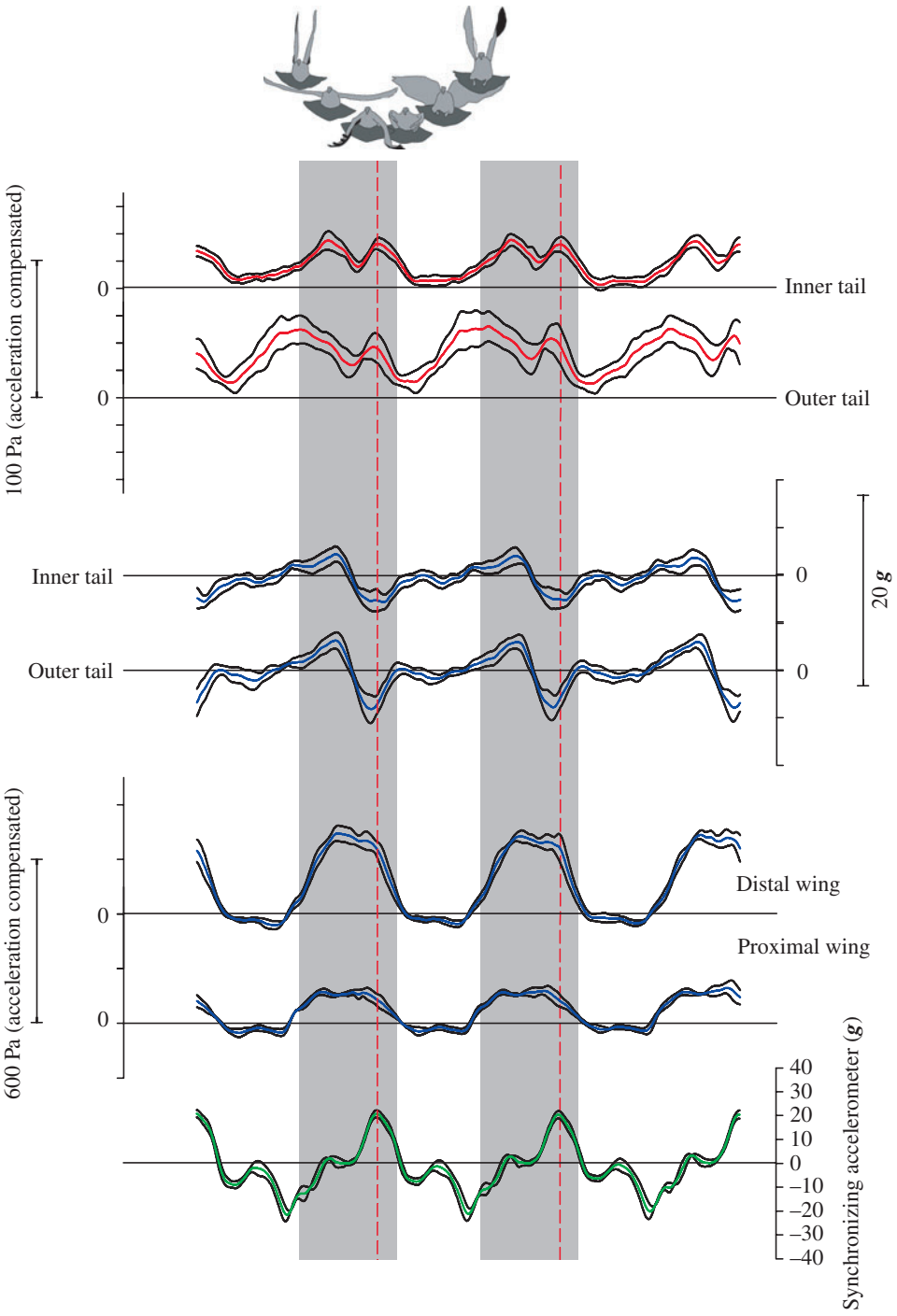


Fig. 5. Mean acceleration-compensated differential pressures for inner and outer tail positions, and distal and proximal wing positions. Also included are acceleration signals for inner and outer tail positions (second pair of traces) and the proximal wing position – the synchronising accelerometer. Tracings of the pigeon through the wing stroke cycle match the timing of the graph. Values are mean ±1 S.D. (shown in black; *N*=3 pigeons). The vertical red broken lines show the relationship between a peak in both inner and outer tail pressure signal, an upwards acceleration of the wings towards the end of downstroke, and a concurrent downwards acceleration of the tail.

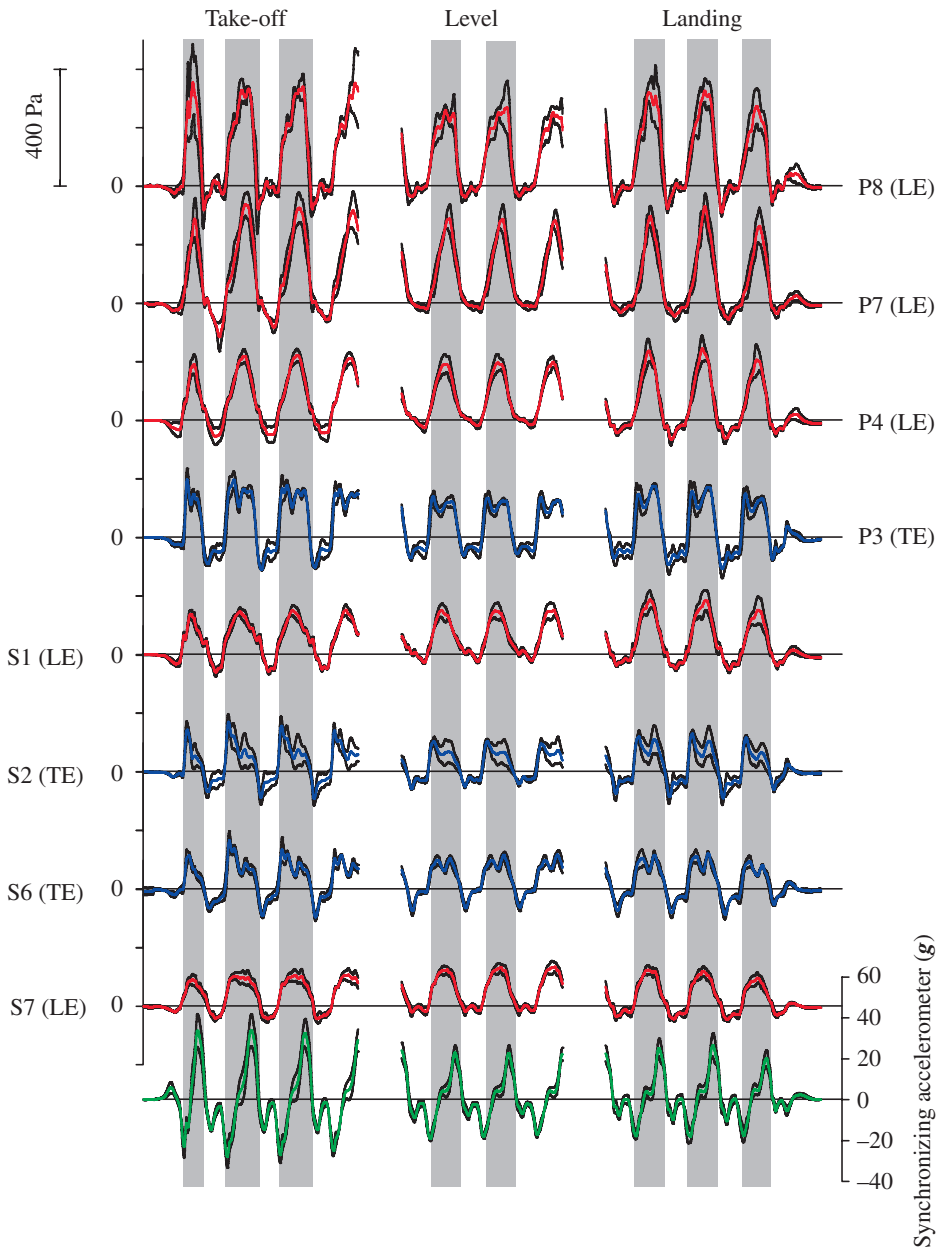


Fig. 6. Mean non-acceleration-compensated differential pressure signals for eight positions (P8, P7, P4, P3, S1, S2, S6, S7) along and across the wing. The traces are ordered from distal sites at the top towards proximal sites nearer the bottom, and the synchronising accelerometer trace again appears as the last trace, in green. Values are mean ±1 S.D. (shown in black; *N*=3 pigeons). Signals for the five sites near the leading edge of the wing are shown in red. Signals for the three pressure sites towards the trailing edge are shown in blue. Periods of downstroke defined by kinematic observations of the wrist are shown as grey for two of the middle three flaps. This shows the close relationship between downstroke timing and the development of 'positive' (ventral-to-dorsal) differential pressures, which are used to define downstroke periods shown with underlying grey boxes for take-off and landing. LE, leading edge; TE, trailing edge.

acceleration. This downwards acceleration of the tail is consistently linked to the second pressure peak measured across the tail, suggesting that the tail is acting as an accelerating plate, and the pressure may be due to accelerating a 'virtual' or 'added' mass of air (e.g. Osborne, 1951).

One implication of the second pressure peak experienced by the tail towards the end of downstroke is the possibility that the tail may act to convert some of the inertial power required to slow the wings (Hedrick et al., 2004) into useful aerodynamic work. Without the tail, the deceleration of the wings at the end of downstroke would result in a downwards acceleration of the body (recorded by the accelerometers at the tail base), and both the body mass and the wing masses would accelerate with respect to the centre of mass. If the aerodynamic forces from the tail limit this reaction-acceleration of the body, the internal work is reduced, and energy is given to the air, potentially providing a useful aerodynamic force and power. To confirm this possibility, detailed changes in tail orientation and velocity through the wing stroke cycle have to be related to the differential pressures, but this is beyond the accuracy of the current techniques.

The tail may have multiple functions during slow flight, and these functions are likely to change as flight speed increases. While a large, widely spread tail may be beneficial during slow flight due to contributing somewhat to weight support, other functions may dominate during slow flight in pigeons. These potentially include a reduction of vertical body oscillations leading to more effective motion of the wings through the air, a conversion of some inertial power to aerodynamic, and a readiness for low-speed manoeuvring.

### *Wing aerodynamic mechanisms*

Sites nearer the leading edge of the wing display approximately half-sinusoidal waveforms during downstroke, while sites nearer the trailing edge exhibit a double peak during downstroke (Fig. 7), similar to that described for distal positions of a goose wing during take-off flight (Usherwood et al., 2003). We suggest that this phenomenon is due to the distance of the sensor from the axis of rotation of the wing during pronation and supination. In our study of Canada goose take-off flight, the distal sites that were sampled on the wing may have been

confounded with more caudal positioning of the pressure sensors. The pressure signal for sites near the trailing edge are interestingly similar to the force traces produced by models of hovering insects (e.g. Dickinson et al., 1999; Birch and Dickinson, 2003). Using their 'robofly' model, Birch and Dickinson (2003) showed that the peak towards the end of the half-stroke (i.e. downstroke or upstroke) is related to an increase in the angle of incidence of the wing. We suggest that, for the pigeons sampled here, the peak in differential pressure for sites nearer the trailing edge during the end of each half-stroke may be due to an increased velocity of the trailing edge during wing rotation prior to the change in wing direction. This would occur due to the distance of the trailing edge sites from the centre of longitudinal rotation of the wing. Whether this results in an increase on the net force for the whole section, however, is unclear.

Our account for the pressure peak towards the ends of each half stroke cannot explain the peaks observed towards the trailing edge at the start of downstroke, because pronation at the start of downstroke would result in a lower velocity at the trailing edge, away from the axis of pronation. In our study of goose wing pressures during take-off flight (Usherwood et al., 2003), we argued that the early peak might be related to an initiation of the downstroke before the wings are fully pronated, resulting in a higher angle of incidence and an increased pressure differential across the wing chord. However, we did not observe this increase in differential pressure at the sites near the leading edge of the pigeon wings in this study. In the case of a scaled, mechanical 'hovering' *Drosophila*, Birch and Dickinson (2003) show that the first peak of each half-stroke can be attributed to a wing–wake interaction. For the pigeons studied here, we propose that a similar wing–wake interaction may be the cause of the significant, earlier peak during each half-stroke by the trailing-edge sites. Although the pigeons were not hovering, their

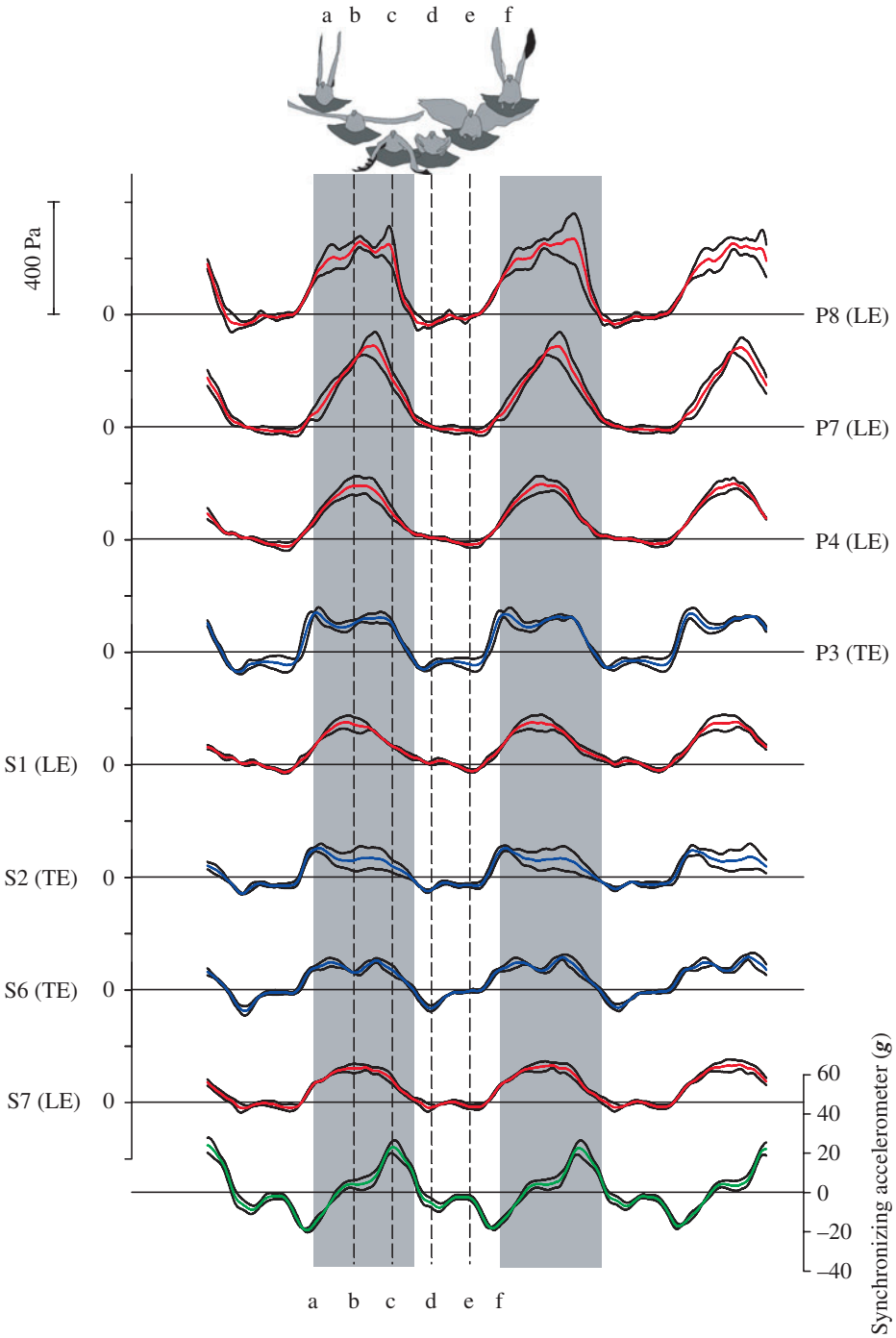


Fig. 7. Expansion of Fig. 6 for the middle three flaps: non-acceleration-compensated pressures for eight sites (P8, P7, P4, P3, S1, S2, S6, S7) along and across the wing. Six pigeon outlines relate to the same timing as the plots, and are labelled a–f. Each tracing is separated in time by an interval of approximately 16 ms (although the rest of the timing remains normalised to the cycle as defined by the synchronising accelerometer peaks). Positions (a) and (f) are the upstroke/downstroke transition, and occur just after the trough in synchronising accelerometer signal. Position (b) indicates mid downstroke, a period of little wing acceleration, coinciding with peak pressure for sites along the leading edge. Position (c) is towards the end of downstroke, when the synchronising accelerometer is being accelerated upwards. Position (d) relates to a downwards acceleration of the proximal wing, after which the distal wing opens up (position e), completing upstroke. LE, leading edge; TE, trailing edge.

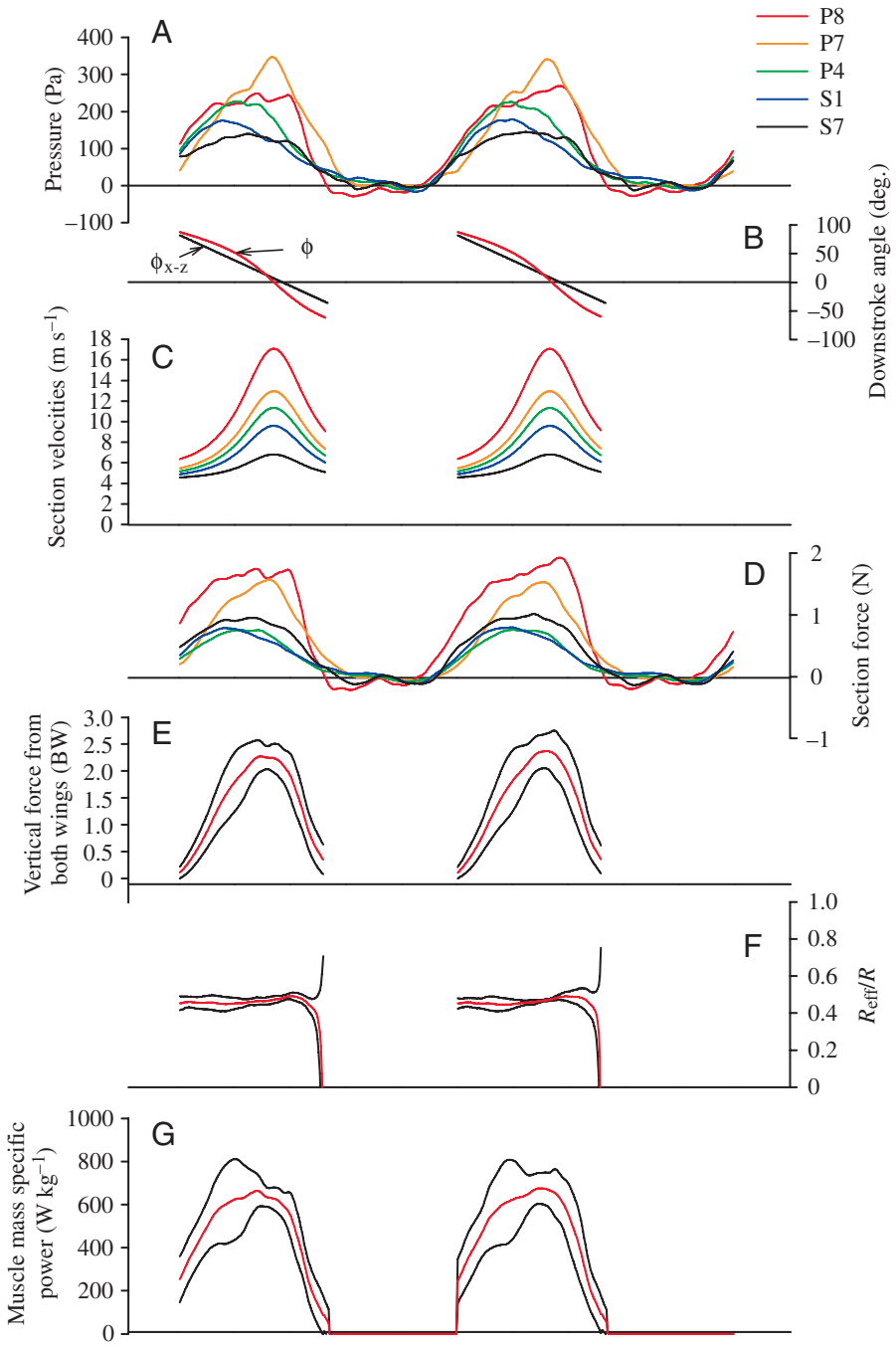


Fig. 8. The implications of the differential pressure measurements of the five sites towards the leading edge of the wing (P8, P7, P4, S1 and S7), and the downstroke kinematics, during the earlier two of the middle three flaps (complete flap cycles are required). (A) Differential pressures. (B) The variation in wing stroke angle during downstroke within the $x$–$z$ plane, i.e. when observed from front-on ($\phi_{x\text{-}z}$), is shown in black, the angle within the stroke plane ($\phi$) in red. (C) The calculated geometric velocity (including forward flight speed) for each wing section. Mean section forces assuming that the measured point pressures can be taken as mean pressures for relevant wing sections of known area (D) are combined, and their orientations to the vertical are taken into account when calculating contribution to weight (BW) support (E). The effective moment arm for the aerodynamic force on the wing ($R_{eff}$), or the effective centre of pressure, acts approximately half way along the wing (F). Instantaneous muscle-mass specific powers (G) are calculated assuming that the pectoralis dominates downstroke power, and constitutes 18% of body mass. Means ± S.D. for weight support, effective moment arm and powers, are calculated from appropriate individual average measurements of differential pressure, kinematics and morphology; averaging is performed as the final step.

advance ratios were low enough (0.38 for the wing tip during downstroke) that an interaction between the wing and the flow due to the previous half-stroke seems likely, and may be expected to influence the pressures across the wing as it starts to flap. Given that the trailing edge sites, unlike the sites at the feather bases, experience pressure differentials right up to the end of each half-stroke, a sudden change in direction at the start of each half-stroke could result in a local interaction with the fluid that had been accelerated by the passing of the wing a moment before. To confirm whether this mechanism acts on the trailing-edge sites of the wing would require flow visualisation similar to that described for hovering model *Drosophila* analysed by Birch and Dickinson (2003). However, such observations of very near-field flow would be very difficult to achieve on live birds.

### *Point pressure measurements and weight support*

Despite certain assumptions, we believe that the calculation of the vertical component of the aerodynamic forces experienced by the wings from our direct differential pressure recordings is fairly robust. On average, a mean vertical force of 74.5% of the body weight was calculated during the level portion of the animal's flight (Table 4). With the additional 7.9% of weight support achieved from tail lift (Table 2) this leaves a deficit of 17.6% of body weight support. Some of this deficit may be attributed to body lift, as well as inaccuracy in our pressure or kinematic measurements, or some failure in the assumptions used in the calculation. In particular, our assumption that a point pressure should represent the mean pressure for a wing section should be treated with caution. Pressure profiles around wing chords rarely show an even pressure distribution. However, our pairs of measurements at similar spanwise positions (P4 and P3; S1 and S2; S6 and S7),

Table 4. *Muscle-mass specific aerodynamic powers – wing results*

| | Cycle powers (weight support 74.5±7.7%) | | | | | |
|---|---|---|---|---|---|---|
| | For both wings | | | For a single wing or pectoralis | | |
| | Aerodynamic power (W) | Body-mass specific power (W kg$^{-1}$) | Muscle-mass specific power (W kg$^{-1}$) | Peak force on a wing (N) | Peak force on a pectoralis (N) | Peak pectoralis stress (kNm$^2$) |
| Method for power calculation | | | | | | |
| Direct measurements: mean kinematics and 5-site pressure map applied to 3 pigeons | 25.6±3.8 | 51.2±5.1 | 272.7±26.7 | 5.7 | 59.0 | 74.1 |
| Induced power | 6.59 | 14.3 | 79.5 | | | |

Induced power is calculated following Pennycuick (1989) with the mean wing span and mass from Table 3 and flight speed from Table 2. The induced power factor $k$ is taken as its default value of 1.2. Muscle-mass specific powers are calculated assuming that the pectoralis dominates downstroke power and constitutes 18% of body mass. Muscle force and stress are calculated using the wing geometry (specifically the shoulder to delto-pectoral crest distance and the cross section of the pectoralis) from pigeons used in other studies (Dial and Biewener, 1993; Biewener et al. 1998; Soman et al., 2005) scaled to the mean body mass of the wild-type pigeons used here, for which a value of 7.385 cm$^2$ was used for the physiological cross-sectional area of the muscle. These values, therefore, should be considered approximate.

while showing somewhat different waveforms, exhibit similar general magnitudes in peak differential pressure (Fig. 6), or time integral of pressure during downstroke, suggesting that the exact chordwise placements may not be critical. We therefore feel that an account of 82.4% of body weight from direct pressure measurements of the wings and tail provides some confidence in the use of differential pressure sensors for determining section force contributions, and justifies our development of a novel method for the calculation of aerodynamic powers.

*Aerodynamic powers from point pressure measurements*

The results for the distribution of section forces exerted on the wing show that the effective moment arm for the aerodynamic force on the wing, or the effective centre of pressure, acts approximately half way along the wing (Fig. 8F). This reflects the fact that the higher differential pressures recorded at more distal sites are offset by their narrower chords. The constancy of $R_{eff}/R$=0.5 throughout the downstroke suggests that lift coefficients vary for each wing position through time; otherwise, the centre of pressure should become biased towards the wing tip at mid-downstroke, when the wing tip is moving relatively fast (Fig. 8C). While the measurement of $R_{eff}/R$ is somewhat limited by the distribution of the pressure sensors, direct pressure measurements allow the assumption of constant spanwise lift and drag coefficients (common in blade-element analyses of slow and hovering flight; see Dickson and Dickinson, 2004) to be avoided.

The mean muscle-mass specific power for a complete flap cycle of 272.7 W kg$^{-1}$ is high compared with both theoretical analyses and previous direct measurements of pectoralis muscle power output obtained using deltopectoral crest (DPC) bone strain measurements and sonomicrometry (discussed below). The muscle-specific induced power requirement (the power associated with changing the momentum of a finite mass of air) for a fixed-wing flier with the flight speed, wingspan, and weight shown in Tables 2 and 3 (using the default induced power factor $k$ of 1.2 and following Pennycuick, 1989) is only 79.5 W kg$^{-1}$. This suggests that induced power is only responsible for 29% of the aerodynamic power requirements of slow flight in pigeons. Thus, our measurements indicate that the pigeon wings experience a very high profile drag, and that induced power is only a relatively small component of the aerodynamic power requirements of *slow* flight (when it is conventionally expected to dominate).

Given the high profile drag coefficients observed for bird wings (Usherwood and Ellington, 2002b) when operating at high incidences and high force coefficients (appropriate for slow flight, especially when profile drag forces contribute to weight support), the dominance of profile power is perhaps not surprising. Indeed, the view of the profile drag coefficient as being some simple, low, and even constant, value is questionable for analyses of the power requirements of bird flight, as has been identified for calculations of the power requirements of insect hovering (Ellington, 1999). Thus, power calculations using profile drag coefficients for steady, attached flow are likely to vastly underestimate power requirements for rapidly flapping flight.

The values of muscle-mass specific aerodynamic power calculated in more theoretical analyses of pigeons in slow flight by Pennycuick (1968) and Rayner (1979b) of 110 W kg$^{-1}$ and 87 W kg$^{-1}$, respectively, are close to the induced powers alone but are markedly lower than the 273 W kg$^{-1}$ calculated in this study. This supports the suggestion that profile drag coefficients conventionally derived from studies involving attached (pre-stall) flow may be misleading. A ‘rule of thumb’ profile drag coefficient of 0.02 is often used (e.g. Askew et al., 2001; following Rayner, 1979a; Pennycuick et al., 1992), which would make profile power relatively insignificant for slow flight. With profile drag coefficients for revolving bird wings potentially >2 (Usherwood and Ellington, 2002b), and the direct aerodynamic power calculations presented here, an undiscriminating use of $C_{Dpro}$=0.02 now appears to be inappropriate.

The value of muscle-mass specific power of 273 W kg$^{-1}$ (for the pectoralis) appears physiologically reasonable, but is higher than the value of 207 W kg$^{-1}$ recently quantified for the pectoralis of White Carneau pigeons flying under nearly identical conditions (Soman et al., 2005), based on DPC strain measurements and detailed muscle sonomicrometry. It is also much higher than the value of 108 W kg$^{-1}$ reported in an earlier study by Biewener et al. (1998) for Silver King pigeons flying at slightly faster free-flight speeds (6–7 m s$^{-1}$). The lower values obtained from measurements of DPC strain, however, may reflect difficulties with aspects of calibration of the *in vivo* technique (see Tobalske et al., 2003). The *in situ* 'pull' calibrations applied to the whole muscle beneath its attachment to the DPC may produce a greater bending moment compared with the *in vivo* distribution of force transmitted by the pectoralis to the DPC. Adopting an aerodynamic correction for estimates of pectoralis power based on DPC strain–force measurements, Tobalske et al. (2003) observed pectoralis mass-specific power outputs that ranged from 80 to 150 W kg$^{-1}$ for cockatiels *Nymphicus hollandicus* and ringed-turtle doves *Streptopelia risoria* flying at 3–5 m s$^{-1}$ in a wind tunnel.

Some uncertainty similarly exists in our estimate of muscle power based on direct wing pressure recordings, which depend on assumptions about both the pressure distributions and the orientation of net aerodynamic forces across a limited number of wing sections. Nevertheless, these measurements indicate that peak forces due to aerodynamics of ~5.7 N are centred halfway down the wing (see Fig. 8), which implies a peak pectoralis force of 59 N and a peak pectoralis stress of 79.9 kN m$^{-2}$ (calculated based on muscle fibre area of 7.39 cm$^2$, given muscle parameters and bone geometries for pigeons used in previous studies; Dial and Biewener, 1993; Biewener et al., 1998). Again, these values are physiologically reasonable but higher than those previously measured *in vivo* in smaller wild-type (Dial and Biewener, 1993) and Silver King pigeons (Biewener et al., 1998) under similar flight conditions. The lower values of peak muscle force and power output obtained from calibrated measurements of strain recorded at the deltopectoral crest, however, may reflect difficulties with aspects of the calibration of the *in vivo* technique (see Tobalske et al., 2003).

While the brief pigeon flights described in this study are unlikely to be near maximal efforts – the pigeons were capable of 80–100 flights in a day with no apparent loss of performance – we do not expect the pigeon flight to be entirely aerobic. Burst muscle-specific powers have been calculated for quail in rapid ascending take-off flight (Askew et al., 2001). Without *any* aerodynamic assumptions, simply calculating the rate of change of potential energy, these flights reach 315 W kg$^{-1}$, and the total aerodynamic power for the quail is likely to be considerably above this value. Thus, our measured values for the power requirements of pigeon flight do not appear extreme, lending some support to the technique. In addition, this suggests that more anaerobic, near-maximal pigeon muscle performances may be studied with a development of the current technique for ascending flight, or loaded flight experiments, and higher calculations of pigeon muscle powers may be expected in the future.

While our calculations of the aerodynamic power requirements for slow, level flight in pigeons are considerably above those derived from both aerodynamic models and *in vivo* muscle measurements, we believe that each component for the power calculation is reasonable. (1) Pressures are low at start and end of the downstroke and high at mid downstroke; (2) net wing forces are close to those required for weight support; (3) wing kinematics are sensible (Table 3) and match those of recent 3-D kinematic measurements of wing stroke plane and amplitude (B. W. Tobalske, T. L. Hedrick and A. A. Biewener, unpublished); and (4) the position of the centre of pressure (the effective moment arm length) occurs approximately half way along the wing (Fig. 8). While a variety of additional aspects may be considered in the calculation of power requirements – for instance additional forces and motions outside the $x$–$z$ plane, or a multiplication factor to scale the forces to support body weight exactly – most of these additions contribute complications that appear to us to be unjustified at this stage, and would indicate even higher power requirements. Thus, we conclude that slow, level flight in pigeons is energetically demanding, and aerodynamically inefficient.

### *Future work*

The direct pressure measurements along and across flapping bird wings reported here for pigeons and previously for Canada geese during take-off flight (Usherwood et al., 2003) have the potential to contribute significantly to the understanding of many aspects of bird flight. The aerodynamic implications of both wing morphology and kinematics can be determined with pressure sensors on bird wings of diverse species flying with a variety of flight styles. Telemetered or data-logged pressure data have the potential to provide insight into the aerodynamic contributions to the physiological implications of free-flight behaviours such as foraging and migration (e.g. following Bishop et al., 2002), or specific flight strategies such as formation flying (following Weimerskirch et al., 2001) or dynamic soaring (Weimerskirch et al., 2000).

## List of symbols

| | |
|---|---|
| $b$ | wing span |
| $C_D$ | drag force component |
| $C_L$ | lift force comoponent |
| $C_R$ | resultant force coefficient |
| dP | differential pressure |
| ds | downstroke |
| $f$ | frequency |
| $F$ | force |
| $F'$ | section force |
| $\boldsymbol{g}$ | gravity |
| $k$ | induced power factor |
| $m$ | loaded mass |
| P | primary feather |
| $P$ | power |

| | |
|---|---|
| $r$ | distance from shoulder |
| R | retrice (tail feather) |
| $R$ | wing length (centre of pressure) |
| $R_{\text{eff}}$ | effective moment arm |
| S | secondary feather |
| $S$ | area |
| $t$ | time |
| $T$ | period |
| $V$ | flight velocity |
| $\alpha$ | angle |
| $\beta$ | inclination of the stroke plane |
| $\phi$ | downstroke angle |
| $\rho$ | density |

We would like to acknowledge the work of Pedro Ramirez for caring for the pigeons, and the help of all at the Field Station during the experiments.

## References

**Alexander, R. McN.** (1968). *Animal Mechanics.* Seattle: University of Washington Press.

**Askew, G. N., Marsh, R. L. and Ellington, C. P.** (2001). The mechanical power output of the flight muscles of the blue-breasted quail (*Coturnis chinensis*) during take-off. *J. Exp. Biol.* **204**, 3601-3619.

**Biewener, A. A., Corning, W. R. and Tobalske, B. W.** (1998). *In vivo* pectoralis muscle force–length behavior during level flight in pigeons (*Columba livia*). *J. Exp. Biol.* **201**, 3293-3307.

**Birch, J. M. and Dickinson, M. H.** (2003). The influence of wing–wake interactions on the production of aerodynamic forces in flapping flight. *J. Exp. Biol.* **206**, 2257-2272.

**Bishop, C. M., Ward, S., Woakes, A. J. and Butler, P. J.** (2002). The energetics of barnacle geese (*Branta leucopsis*) flying in captive and wild conditions. *Comp. Biochem. Physiol.* **133A**, 225-237.

**Dial, K. P. and Biewener, A. A.** (1993). Pectoralis-muscle force and power output during different modes of flight in pigeons (*Columba livia*). *J. Exp. Biol.* **176**, 31-54.

**Dickinson, M. H.** (1996). Unsteady mechanisms of force generation in aquatic and aerial locomotion. *Am. Zool.* **36**, 536-554.

**Dickinson, M. H., Lehmann, F.-O. and Sane, S. P.** (1999). Wing rotation and the aerodynamic basis of insect flight. *Science* **284**, 1954-1960.

**Dickson, W. B. and Dickinson, M. H.** (2004). The effect of advance ratio an the aerodynamics of revolving wings. *J. Exp. Biol.* **207**, 4269-4281.

**Ellington, C. P.** (1984). The aerodynamics of hovering insect flight. V. A vortex theory. *Phil. Trans. R. Soc. Lond. B* **305**, 115-144.

**Ellington, C. P.** (1999). The novel aerodynamics of insect flight: applications to micro-air vehicles. *J. Exp. Biol.* **202**, 3439-3448.

**Ellington, C. P., Van den Berg, C., Willmott, A. P. and Thomas, A. L. R.** (1996). Leading-edge vortices in insect flight. *Nature* **384**, 626-630.

**Hedrick, T. L., Tobalske, B. W. and Biewener, A. A.** (2002). Estimates of circulation and gait change based on a three dimensional kinematic analysis of flight in cockatiels (*Nymphicus hollandicus*) and ringed turtle-doves (*Streptopelia risoria*). *J. Exp. Biol.* **205**, 1389-1409.

**Hedrick, T. L., Tobalske, B. W. and Biewener, A. A.** (2003). How cockatiels (*Nymphicus hollandicus*) modulate pectoralis power output across flight speeds. *J. Exp. Biol.* **206**, 1363-1378.

**Hedrick. T. L., Usherwood, J. R. and Biewener, A. A.** (2004). Wing inertia and whole-body acceleration: an analysis of instantaneous aerodynamic force production in cockatiels (*Nymphicus hollandicus*) flying across a range of speeds. *J. Exp. Biol.* **207**, 1689-1702.

**Liu, H., Ellington, C. P., Kawachi, K., Van den Berg, C. and Willmott, A. P.** (1998). A computational fluid dynamic study of hawkmoth hovering. *J. Exp. Biol.* **201**, 461-477.

**Liu, H. and Kawachi, K.** (1998). A numerical study of insect flight. *J. Comput. Phys.* **146**, 124-156.

**Osborne, M. F. M.** (1951). Aerodynamics of flapping flight with application to insects. *J. Exp. Biol.* **28**, 221-245.

**Pennycuick, C. J.** (1968). Power requirements for horizontal flight in the pigeon *Columba livia*. *J. Exp. Biol.* **49**, 527-555.

**Pennycuick, C. J.** (1975). Mechanics of flight. In *Avian Biology*, vol. 5 (ed. D. S. Farner and J. R. King), pp. 1-75. London: Academic Press.

**Pennycuick, C. J.** (1989). *Bird Flight Performance: a Practical Calculation Manual.* Oxford: Oxford University Press.

**Pennycuick, C. J., Heine, C. E., Kirkpatrick, S. J. and Fuller, M. R.** (1992). The profile drag coefficient of a Harris' hawk wing, measured by wake sampling in a wind tunnel. *J. Exp. Biol*. **165**, 1-19.

**Ramamurti, R. and Sandberg, W. C.** (2002). A three-dimensional computational study of the aerodynamic mechanisms of insect flight. *J. Exp. Biol*. **205**, 1507-1518.

**Rayner, J. M. V.** (1979a). A vortex theory of animal flight. Part 2. The forward flight of birds. *J. Fluid Mech.* **94**, 731-763.

**Rayner, J. M. V.** (1979b). A new approach to animal flight mechanics. *J. Exp. Biol.* **80**, 17-54.

**Rayner, J. M. V.** (1993). On the aerodynamics and the energetics of vertebrate flapping flight. *Cont. Math.* **141**, 351-400.

**Sane, S. P.** (2003). The aerodynamics of insect flight. *J. Exp. Biol.* **206**, 4191-4208.

**Soman, A., Hedrick, T. L. and Biewener, A. A.** (2005). Regional patterns of pectoralis fascicle strain in the region *Columba livia* during level flight. *J. Exp. Biol.* **208**, in press.

**Spedding, G. R.** (1986). The wake of a jackdaw (*Corvus monedula*) in slow flight. *J. Exp. Biol.* **125**, 287-307.

**Spedding, G. R.** (1987). The wake of a kestrel (*Falco tinnunculus*) in flapping flight. *J. Exp. Biol.* **127**, 59-78.

**Spedding, G. R., Rayner, J. M. V. and Pennycuick, C. J.** (1984). Momentum and energy in the wake of a pigeon (*Columba livia*) in slow flight. *J. Exp. Biol.* **111**, 81-102.

**Spedding, G. R., Rosén, M. and Hedenström, A.** (2003a). A family of vortex wakes generated by a thrush nightingale in free flight in a wind tunnel over its entire natural range of flight speeds. *J. Exp. Biol.* **206**, 2313-2344.

**Spedding, G. R., Rosén, M. and Hedenström, A.** (2003b). Quantitative studies of the wakes of freely-flying birds in a low-turbulence wind tunnel. *Exp. Fluids* **34**, 291-303.

**Sun, M. and Tang, J.** (2002). Unsteady aerodynamic force generation by a model fruit fly wing in flapping motion. *J. Exp. Biol.* **205**, 55-70.

**Tobalske, B. W., Hedrick, T. L., Dial, K. P. and Biewener, A. A.** (2003). Comparative power curves in bird flight. *Nature* **421**, 363-366.

**Usherwood, J. R. and Ellington, C. P.** (2002a). The aerodynamics of revolving wings. I. Model hawkmoth wings. *J. Exp. Biol.* **205**, 1547-1564.

**Usherwood, J. R. and Ellington, C. P.** (2002b). The aerodynamics of revolving wings. II. Propeller force coefficients from mayfly to quail. *J. Exp. Biol.* **205**, 1565-1576.

**Usherwood, J. R., Hedrick, T. L. and Biewener, A. A.** (2003). The aerodynamics of avian take-off from direct pressure measurements in Canada geese (*Branta canadensis*). *J. Exp. Biol.* **206**, 4051-4056.

**Van den Berg, C. and Rayner, J. M. V.** (1995). The moment of inertia of bird wings and the inertial power requirement for flapping flight. *J. Exp. Biol.* **198**, 1655-1664.

**Wakeling, J. M. and Ellington, C. P.** (1997). Dragonfly flight. III. Lift and power requirements. *J. Exp. Biol.* **200**, 583-600.

**Wang, Z. J.** (2000). Two dimensional mechanism for insect hovering. *Phys. Rev. Lett.* **85**, 2216-2219.

**Weimerskirch, H., Martin, J., Clerquin, Y., Alexandre, P. and Jiraskova, S.** (2001). Energy saving in flight formation. *Nature* **413**, 697-698.

**Weimerskirch, H., Guionnet, T., Martin, J., Shaffer, S. A. and Costa, D. P.** (2000). Fast and efficient? Optimal use of wind by flying albatrosses. *Proc. R. Soc. B* **267**, 1869-1874.